Lightweight 2D Imaging for Integrated Imaging and Communication Applications

Xiaohua Li , *Senior Member, IEEE*, and Yu Chen , *Senior Member, IEEE*

Abstract—While integrated sensing and communication has attracted great attention, integrated imaging and communication is still largely open. Microwave, millimeter-wave, and tera-Hz imaging needs to sample a huge number of antenna positions and is thus too complex and costly to mobile communication devices. To address this challenge, we propose a Lightweight Imaging Algorithm (LIA) to reduce the complexity of both imaging hardware and computation. Based on the synthetic aperture radar principle, LIA uses the iterative matrix inversion lemma to estimate image pixels efficiently. Simulations with both simulated and real-world data verified that LIA had superior performance. The algorithm is promising to compact handheld and mobile devices in integrated imaging and communication applications.

Index Terms—5G cell system, integrated sensing and communication, iterative matrix inversion, millimeter-wave imaging.

I. INTRODUCTION

INTEGRATED sensing and communication, where sensing and communication share the same frequency and hardware [1], has been considered as a killer application for the fifth-generation (5G) and beyond cellular communication systems. It has been studied extensively in joint radar and communication systems [2]–[4], autonomous vehicles and unmanned aerial vehicles (UAV) [5]–[7], smart home and senior care [8]–[10], security and surveillance [11]–[13], etc. Nevertheless, existing works are limited to radar sensing functions only, i.e., detecting the target's range, speed, and angle. In many important applications such as senior care and surveillance, the imaging function, i.e., providing high-resolution images of the target similar to optical cameras, is highly needed.

Microwave, millimeter-wave (mmWave), and Tera-Hertz (THz) imaging can provide high-resolution images and has been used widely in airport screening [14], [15], medical imaging [16], concealed weapon detection [17], [18], etc. It has the unique advantage of overcoming many challenging issues associated with optical cameras, such as difficulties caused by weather (i.e. at night, in foggy weather, or on rainy days), environment (i.e. blockage behind wall, curtain, or clothes), and privacy concerns [19], [20]. With the adoption of mmWave
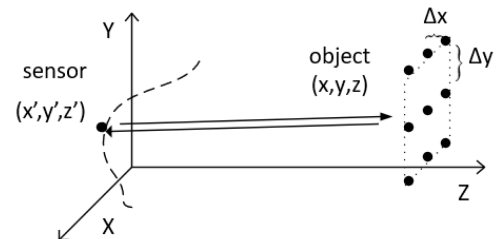
Fig. 1. A mobile sensor images a target.

and THz in 5G and beyond systems, integrated imaging and communication has a high potential in security, medical, and industrial applications.

To the best of our knowledge, integrated imaging and communication is still an open problem. One of the primary reasons is that imaging is too complex and costly to mobile communication devices. It requires bulky antenna arrays, either physical arrays or virtual arrays realized by scanning a large number of antenna positions. Although desperately needed, the compact handheld imaging device is still not available [15]. A sparse array used 736 transmit (Tx) antennas and 736 receive (Rx) antennas to electronically scan 25 600 antenna positions within a 50 cm × 50 cm aperture [21]. Another sparse array used 480 Tx antennas and 480 Rx antennas to scan 36 864 antenna positions within a 100 cm × 100 cm aperture [22]. A sensor with a single Tx and a single Rx antenna was moved mechanically to sample 512×512 antenna positions within a 25 cm × 25 cm aperture [18]. It took more than 10 minutes to finish a full scan. Similarly, a sensor was moved over a 40 cm × 40 cm two-dimensional (2D) rail with a step size of 0.1 cm in each dimension [23]. This kind of scan over a 2D regular grid is unrealistic to handheld or mobile imagers.

To address the challenge, we develop a Lightweight Imaging Algorithm (LIA) that makes 2D imaging affordable to handheld devices. The algorithm is lightweight in both hardware and computation as it does not need regular-grid antenna arrays and has low computational complexity. In contrast, some recent work explored the microwave metasurface technology to reduce hardware and computational complexity [24]. The rest of this letter is organized as follows. The signal model is presented in Section II. The new algorithm is developed in Section III. Simulations and conclusions are given in Sections IV and V, respectively.

II. SIGNAL MODEL

As illustrated in Fig. 1, a sensor moves along a trajectory $\mathbf{r}' = (x', y', z')$ while imaging a target located at $\mathbf{r} = (x, y, z)$. We

assume the sensor has a single Tx antenna and a single co-located Rx antenna. It transmits signal $p(t)$ with carrier frequency f_c, and receives the signal $\hat{s}_{\mathbf{r}'}(t)$ reflected by the target, i.e.,

$$\hat{s}_{\mathbf{r}'}(t) = \int_{\mathbf{r}} \sigma_{\mathbf{r}} p(t - \tau_{\mathbf{r}'\mathbf{r}}) d\mathbf{r} + \hat{v}_{\mathbf{r}'}(t), \qquad (1)$$

where $\tau_{\mathbf{r}'\mathbf{r}}$ is the propagation delay, $\sigma_{\mathbf{r}}$ is the target's reflection coefficient, and $\hat{v}_{\mathbf{r}'}(t)$ denotes noise, interference, and clutter [25]. With the signal processing outlined in the Appendix, we get a data sample at each antenna position $\mathbf{r}'$ as

$$s_{\mathbf{r}'} = \int_{\mathbf{r}} \sigma_{\mathbf{r}} e^{j 2\pi f_c \tau_{\mathbf{r}'\mathbf{r}}} d\mathbf{r} + v_{\mathbf{r}'}, \qquad (2)$$

where $v_{\mathbf{r}'}$ denotes the processed $\hat{v}_{\mathbf{r}'}(t)$.

For 2D imaging, we assume the target has a fixed $z = z_0$ and would like to reconstruct an $I \times J$ target image $\mathbf{X}$ with pixel $X_{ij} = \sigma_{\mathbf{r}} \Delta x \Delta y$, where $\mathbf{r} = (x, y, z_0)$ is discretized as $x = i\Delta x + x_0$, $y = j\Delta y + y_0$, $0 \le i \le I - 1$, $0 \le j \le J - 1$, Δx and Δy are discretizing stepsize or imaging resolution, x_0 and y_0 are shifts. We stack the columns of $\mathbf{X}$ into an N dimensional column vector $\mathbf{x} = \mathrm{vec}(\mathbf{X})$, whose nth entry is $x_n = X_{ij}$, $n = jI + i$, and $N = IJ$.

With M samples of data obtained at M antenna positions $\mathbf{r}'_m = (x_m,' y_m,' z_m')$, $m = 0, \ldots, M - 1$, we stack them into an M dimensional column vector $\mathbf{y}$, whose mth element is $y_m = s_{\mathbf{r}'_m}$. Then we have

$$\mathbf{y} = \mathbf{H}\mathbf{x} + \mathbf{v}, \qquad (3)$$

where the element of the $M \times N$ matrix $\mathbf{H}$ is

$$H_{mn} = e^{j 4\pi R_{mn}/\lambda}, \quad 0 \le m \le M - 1, 0 \le n \le N - 1, \quad (4)$$

with $R_{mn} = R_{m,jI+i} = ((x'_m - i\Delta x - x_0)^2 + (y'_m - j\Delta y - y_0)^2 + (z'_m - z_0)^2)^{1/2}$ and λ is the wavelength. The vector $\mathbf{v}$ includes noise, interference, and clutter. This is the general signal model for radar imaging, remote sensing, and medical imaging [16]. Imaging is to estimate $\mathbf{x}$ from known $\mathbf{y}$ and $\mathbf{H}$.

For fixed z', imaging resolution is $\frac{\lambda |z_0 - z'|}{2D}$, where D is the array aperture size in each dimension [18]. High-resolution imaging needs large D, small λ, and close sensor-target distance. Even though not required by (3), almost all the existing 2D imaging studies use dense 2D antenna arrays with regular antenna separation $\lambda/2$, which makes the number of antenna positions $M = (2D/\lambda)^2$ extremely large.

For lightweight imaging, we propose to exploit irregularly-located antenna positions to reduce hardware demand. For example, a user can simply move a handhold sensor such as a mobile phone along an arbitrary trajectory $\mathbf{r}'$ to acquire data samples $s_{\mathbf{r}'_m}$. Cellular base-stations can work collaboratively to construct an irregular sparse array to acquire data.

III. IMAGING ALGORITHMS

A. Limitation of Existing Imaging Algorithms

Solving (3) is nontrivial because of the huge-dimension and ill-condition of $\mathbf{H}$. We cannot directly calculate the inverse of $\mathbf{H}$. Instead, we can minimize $\|\mathbf{y} - \mathbf{H}\mathbf{x}\|^2$ iteratively via

$$\hat{\mathbf{x}}(\ell + 1) = \hat{\mathbf{x}}(\ell) - \mu \mathbf{H}^H (\mathbf{y} - \mathbf{H}\hat{\mathbf{x}}(\ell)), \quad \ell = 0, 1, \cdots \quad (5)$$

where μ is stepsize and $(\cdot)^H$ denotes Hermitian. The computational complexity is $O(MN)$ per iteration. The problem is that

slow convergence makes the total computation workload very high. The calculation of the huge matrix $\mathbf{H}$ in each iteration is especially undesirable. Besides, regularization is often needed to mitigate the ill-condition of $\mathbf{H}$, which further increases computational complexity [16].

Alternatively, following the practice of synthetic aperture radar (SAR), we can apply the computationally efficient back-projection (BP) algorithm [26], [27], which in our case is

$$\hat{\mathbf{x}} = \mathbf{H}^H \mathbf{y}. \qquad (6)$$

The total computational complexity is $O(MN)$ only. It projects the received samples back to the target point, i.e., coherently combines the received samples using the propagation delays in $\mathbf{H}$ as a spatial matched filter. From (3) and (6), one can easily see that an extremely large number of antenna samples, i.e., large M, is needed to make $\mathbf{H}^H\mathbf{H}$ close to the identity. This leads to high hardware complexity.

Instead of using (6) with the huge matrix $\mathbf{H}$, SAR exploits regular 2D sampling and fast Fourier transform (FFT) to reduce computation [25], [28]. Consider a $K \times L$ 2D array with $M = KL$ antenna positions $\mathbf{r}' = (x,' y,' z_0')$, where $x' = k\Delta x' + x_0'$, $y' = \ell\Delta y' + y_0'$, $0 \le k \le K - 1$, $0 \le \ell \le L - 1$, z_0' is fixed, x_0' and y_0' are shifts. We further let $\Delta x' = \Delta x$ and $\Delta y' = \Delta y$. Stack all samples into a $K \times L$ matrix $\mathbf{Y}$ with elements $Y_{k\ell} \triangleq s_{\mathbf{r}'}$. Skipping noise and considering (2) with the discretized $\mathbf{r}'$ and $\mathbf{r}$, we have

$$Y_{k\ell} = \sum_{i=0}^{I-1} \sum_{j=0}^{J-1} X_{ij} e^{j 4\pi R_{k\ell ij}/\lambda}, \qquad (7)$$

where $R_{k\ell ij} = [(k\Delta x + x_0' - i\Delta x - x_0)^2 + (\ell\Delta y + y_0' - j\Delta y - y_0)^2 + (z_0' - z_0)^2]^{1/2}$. We find that (7) is 2D convolution

$$Y_{k\ell} = \sum_{i=0}^{I-1} \sum_{j=0}^{J-1} X_{ij} B_{k-i, \ell-j}, \qquad (8)$$

where $B_{mn} = e^{j 4\pi/\lambda \sqrt{(m\Delta x + x_0' - x_0)^2 + (n\Delta y + y_0' - y_0)^2 + (z_0' - z_0)^2}}$ is the element of a 2D filter $\mathbf{B}$. With 2D FFT, we have $\mathrm{FFT2}(\mathbf{Y}) = \mathrm{FFT2}(\mathbf{X}) \odot \mathrm{FFT2}(\mathbf{B})$ approximately, where $\odot$ is element-wise product. We cannot divide $\mathrm{FFT2}(\mathbf{Y})$ by $\mathrm{FFT2}(\mathbf{B})$ due to the latter's ill condition. Instead, we can apply matched filter and (6) to reconstruct the image as

$$\hat{\mathbf{X}} = \mathrm{IFFT2}\left(\mathrm{FFT2}(\mathbf{Y}) \odot \mathrm{FFT2}(\mathbf{B}^*)\right), \qquad (9)$$

where * is conjugation. This is the matched filter algorithm in [29]. The imaging community more widely uses its equivalent wavenumber domain form [18]. The computational complexity is $O(\max\{M, N\} \log(\max\{M, N\}))$ only. The problem of (9) is that it requires regular 2D sampling that is infeasible for mobile sensors. Both (6) and (9) are not hardware efficient since the performance degrades severely if M is not sufficiently large.

B. Lightweight Imaging Based on Iterative Matrix Inversion

To avoid the hardware challenges of regular 2D arrays, we have to work with (3). For integrated imaging and communication, we need to develop lightweight algorithms that are more efficient than (5) and perform better than (6).

TABLE I
PROPOSED LIA ALGORITHM. $\mathbf{G}_{:\ell}$ AND $\mathbf{G}_{\ell:}$ DENOTE THE ℓTH COLUMN AND
ROW OF THE MATRIX $\mathbf{G}$, RESPECTIVELY

Initialize: $\mathbf{G}(-1) = \delta\mathbf{H}^H\mathbf{H}$, $\tilde{\mathbf{x}}(-1) = \delta\mathbf{H}^H\mathbf{y}$.
Update: for $\ell = 0, \cdots, N-1$,
$\quad\quad\quad \mathbf{g} = \mathbf{G}_{:\ell}(\ell-1)/(1 + \mathbf{G}_{\ell\ell}(\ell-1))$
$\quad\quad\quad \tilde{\mathbf{x}}(\ell) = \tilde{\mathbf{x}}(\ell-1) - \mathbf{g}\tilde{x}_\ell(\ell-1)$
$\quad\quad\quad \mathbf{G}(\ell) = \mathbf{G}(\ell-1) - \mathbf{g}\mathbf{G}_{\ell:}(\ell-1)$
Output: $\hat{\mathbf{x}} = \tilde{\mathbf{x}}(N-1)/\text{diag}(\mathbf{G}(N-1))$

From (3), we estimate image pixels as $\hat{x}_n = \mathbf{f}_n^H\mathbf{y}$, $n = 0, \ldots, N-1$, with vectors $\mathbf{f}_n$ that are optimized from

$$\min \|\mathbf{f}_n^H\mathbf{H}_{-n}\|^2, \quad \text{s.t.,} \quad \mathbf{f}_n^H\mathbf{h}_n = 1, \quad (10)$$

where $\mathbf{H}_{-n} = [\mathbf{h}_0, \ldots, \mathbf{h}_{n-1}, \mathbf{h}_{n+1}, \ldots, \mathbf{h}_{N-1}]$ is the remaining of the matrix $\mathbf{H}$ after knocking out the n-th column $\mathbf{h}_n$. Define $\mathbf{R} = \mathbf{H}\mathbf{H}^H$ and $\mathbf{W} = \mathbf{R}^{-1}$.

Proposition 1: Image pixels can be estimated as

$$\hat{x}_n = (\mathbf{h}_n^H\mathbf{W}\mathbf{h}_n)^{-1}\mathbf{h}_n^H\mathbf{W}\mathbf{y}. \quad (11)$$

Proof: The optimal solution to (10) is

$$\mathbf{f}_n = (\mathbf{h}_n^H\mathbf{R}_n^{-1}\mathbf{h}_n)^{-1}\mathbf{R}_n^{-1}\mathbf{h}_n \quad (12)$$

where $\mathbf{R}_n = \mathbf{H}_{-n}\mathbf{H}_{-n}^H$ [30]. We can calculate $\mathbf{R}_n$ by the matrix inversion lemma to reduce computational complexity and to avoid the explicit inversion of ill-conditioned matrices. Specifically, since $\mathbf{R}_n = \mathbf{R} - \mathbf{h}_n\mathbf{h}_n^H$, we have

$$\mathbf{R}_n^{-1} = \mathbf{R}^{-1} + \mathbf{R}^{-1}\mathbf{h}_n(1 - \mathbf{h}_n^H\mathbf{R}^{-1}\mathbf{h}_n)^{-1}\mathbf{h}_n^H\mathbf{R}^{-1}. \quad (13)$$

It follows that $\mathbf{R}_n^{-1}\mathbf{h}_n = \mathbf{R}^{-1}\mathbf{h}_n(1 - \mathbf{h}_n^H\mathbf{R}^{-1}\mathbf{h}_n)^{-1}$. Putting it into (12), we get (11). ∎

The matrix $\mathbf{W}$ can be evaluated iteratively. Since $\mathbf{R} = \sum_{\ell=0}^{N-1}\mathbf{h}_\ell\mathbf{h}_\ell^H$, we can rewrite it in the iterative form $\mathbf{R}(\ell) = \mathbf{R}(\ell-1) + \mathbf{h}_\ell\mathbf{h}_\ell^H$, $\ell = 0, \ldots, N-1$, with $\mathbf{R}(-1) = \mathbf{0}$ and $\mathbf{R} = \mathbf{R}(N-1)$. Define $\mathbf{W}(\ell) \triangleq \mathbf{R}^{-1}(\ell)$. With the matrix inversion lemma we have

$$\mathbf{W}(\ell) = \mathbf{W}(\ell-1)$$
$$- \mathbf{W}(\ell-1)\mathbf{h}_\ell[1 + \mathbf{h}_\ell^H\mathbf{W}(\ell-1)\mathbf{h}_\ell]^{-1}\mathbf{h}_\ell^H\mathbf{W}(\ell-1). \quad (14)$$

Based on (14) and (11), we can estimate the image. We propose to skip the calculation of the matrix $\mathbf{W}$ and to update pixel estimation directly. Based on (11), define $\tilde{x}_n(\ell) \triangleq \mathbf{h}_n^H\mathbf{W}(\ell)\mathbf{y}$ and $g_{nj}(\ell) \triangleq \mathbf{h}_n^H\mathbf{W}(\ell)\mathbf{h}_j$. Replacing $\mathbf{W}(\ell)$ in $\tilde{x}_n(\ell)$ with (14), we have

$$\tilde{x}_n(\ell) = \tilde{x}_n(\ell-1) - g_{n\ell}(\ell-1)[1 + g_{\ell\ell}(\ell-1)]^{-1}\tilde{x}_\ell(\ell-1). \quad (15)$$

Similarly, replacing $\mathbf{W}(\ell)$ in the definition of $g_{nj}(\ell)$ gives

$$g_{nj}(\ell) = g_{nj}(\ell-1) - g_{n\ell}(\ell-1)[1 + g_{\ell\ell}(\ell-1)]^{-1}g_{\ell j}(\ell-1). \quad (16)$$

After updating $\tilde{x}_n(\ell)$ and $g_{nj}(\ell)$ for $\ell = 0, \ldots, N-1$, from (11) image pixels can be calculated as

$$\hat{x}_n = g_{nn}^{-1}(N-1)\tilde{x}_n(N-1). \quad (17)$$

Equations (15)-(17) lead to the Lightweight Imaging Algorithm (LIA) in Table I, where $\tilde{\mathbf{x}}(\ell) \triangleq [\tilde{x}_0(\ell), \ldots, \tilde{x}_{N-1}(\ell)]^T$, $\hat{\mathbf{x}} \triangleq [\hat{x}_0, \ldots, \hat{x}_{N-1}]^T$, $g_{nj}(\ell)$ is the (n,j)th element of the

$N \times N$ matrix $\mathbf{G}(\ell)$, and $(\cdot)^T$ denotes transpose. $\mathbf{G}(-1)$ and $\tilde{\mathbf{x}}(-1)$ are initialized as the correlation matrix and the BP image (6) with a small attenuation factor δ, respectively.

The computational complexity of the initialization step is $O(MN^2)$. Exploiting the structure of $\mathbf{H}$, we can further reduce the complexity, even to the level of $O(MN)$ with mild approximations. Details are skipped to save space. What is important is that the computational complexity of the updating step is $O(N^3)$ in total, or $O(N^2)$ in each iteration. As a key advantage, the huge matrix $\mathbf{H}$ is used in initialization only and the iterative procedure depends on the number of pixels N only. We often have $M \gg N$ because more antenna samples are always desired while the image size N is adjustable. We can reduce N in practical applications to reduce computational complexity. For example, we can first estimate a coarse image with a small N. Then, according to the image contents, we refocus on a small interesting area to get an image with higher resolution but still small N.

IV. SIMULATIONS

With both simulated and real measured data, we compared **LIA** with three conventional algorithms: Back-Project Algorithm (**BPA**) of (6), Matched Filter Algorithm (**MFA**) with 2D FFT of (9) [29], and Gradient Descent Algorithm (**GDA**) of (5) [16]. The GDA ran N iterations with zero initialization and heuristically optimized μ.

To generate the simulated data, we created a target consisting of five point-sources located on a circle with 5 cm radius. The target was 500 cm away from the sensor that had a single Tx antenna and a single Rx antenna. The sensor moved within a 100 cm × 100 cm square in the x-y plane, which means array aperture $D = 100$ cm. It transmitted mmWave 5G signal with $f_c = 75$ GHz. Imaging resolution was thus 1 cm. We reconstructed images with size $I \times J = 30 \times 30$ for the target area of 10 cm × 10 cm. The BPA, GDA, and our LIA algorithms used random antenna positions, while the MFA had evenly separated antenna positions.

For real data, we used the FMCW-based mmWave radar dataset [23] downloaded from https://utdallas.box.com/s/d88adydix1qhzg0ko3lagqli4jmtofd0. The data were generated by moving a 79 GHz radar sensor across a regular 2D grid with $\Delta x' = \lambda/2$ and $\Delta y' = 2\lambda$. A 5 cm × 7.5 cm metal plate with various holes was placed 28 cm away from the sensor. After FMCW signal processing, we had a $K \times L = 100 \times 407$ data matrix, corresponding to array aperture $D = 20$ cm and imaging resolution 0.27 cm in both dimensions. We focused on a target area of 15 cm × 15 cm, and reconstructed images with size $I \times J = 40 \times 50$. The reference (or true) image was constructed by MFA with all the data. Although both the sensor and the target have fixed z locations in experiments, our LIA does not need z to be fixed.

For the simulated data, Fig. 2 shows the actual target image and two reconstructed images with $M = 4096$ antenna positions. For the real data, Fig. 3 shows the reference image and three images reconstructed by LIA, BPA, and GDA with $M = 4000$, respectively. We can see that our LIA algorithm reconstructed the target images successfully in both cases with only around 4000 irregularly-distributed antenna positions. Although some images were not shown due to space limit, we

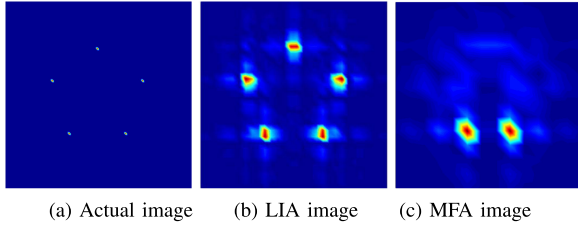(a) Actual image   (b) LIA image   (c) MFA image

Fig. 2. Simulated data. (a) Actual target image. (b) Image reconstructed by our LIA with $M = 4096$ random antenna positions. (c) Image reconstructed by 2DFFT-based MFA with 64×64 regular-spaced antenna positions.

(a) Reference image   (b) LIA image

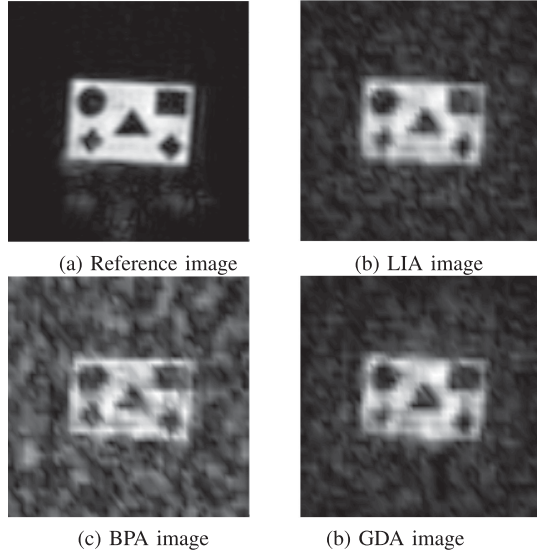(c) BPA image   (b) GDA image

Fig. 3. Real measured data. (a) Reference target image. (b)-(d) Images reconstructed by the LIA, BPA, and GDA algorithms with $M = 4000$ random antenna positions.

TABLE II
IMAGE RECONSTRUCTION PERFORMANCE COMPARISON

	M	Alg.	PSNR (dB)	SSIM	Time (sec)
	1024	MFA	12.0	0.06	0.01
		BPA	17.4	0.04	0.08
		GDA	18.3	0.05	57.79
		LIA	**18.8**	**0.12**	4.51
Simulated Data	4096	MFA	16.1	0.08	0.01
		BPA	18.5	0.06	0.20
		GDA	18.9	0.18	207.74
		LIA	**19.2**	**0.23**	4.75
	65536	MFA	18.9	0.19	0.02
		BPA	18.6	0.17	2.02
		GDA	19.2	0.21	2093.91
		LIA	**19.3**	**0.26**	8.93
	2000	BPA	12.7	0.15	0.89
		GDA	14.1	0.16	127.23
		LIA	**15.3**	**0.19**	53.88
Real Measured Data	4000	BPA	14.5	0.21	1.89
		GDA	20.9	0.39	251.39
		LIA	**22.9**	**0.44**	54.97
	16000	BPA	21.8	0.42	8.09
		GDA	27.0	0.82	968.78
		LIA	**27.1**	**0.83**	63.51

found that the MFA failed while the image quality of BPA and GDA was much worse than LIA.

Image reconstruction quality was compared quantitatively in Table II in terms of peak-signal-to-noise ratio (PSNR) and structural similarity method (SSIM) [31]. The running time for

reconstructing an image was also shown. Our LIA always gave better image quality. It ran much faster than the GDA whose speed was hampered severely by the huge matrix **H** used in each iteration. Although the BPA and MFA were faster, they could not work reliably when M was not big enough. The running time was obtained by running their MATLAB implementations over a computer with an Intel Core i7-8700 CPU. A binary C implementation can make our LIA algorithm faster and closer to BPA.

V. CONCLUSIONS

This letter develops a novel Lightweight Imaging Algorithm (LIA) for 2D imaging with microwave, millimeter-wave, and tera-Hertz signals. The proposed LIA algorithm is lightweight in both hardware and computation. It resolves the challenge that existing imaging algorithms all need large and costly antenna arrays that are infeasible to handheld sensors. Simulations demonstrate its superior performance. The LIA algorithm is promising for integrated imaging and communication applications.

APPENDIX

For integrated imaging and communication, the transmitted signal $p(t)$ can be either communication signal or radar signal. Consider first FMCW (frequency-modulated continuous waveform) signal $p(t) = e^{j2\pi(f_c t + 0.5\beta t^2)}$ with sweeping frequency β. After de-chirping [25] and neglecting noise, the received signal (1) becomes

$$s_{\mathbf{r}'}(t) = \int_{\mathbf{r}} \sigma_{\mathbf{r}} e^{j2\pi(f_c \tau_{\mathbf{r}'\mathbf{r}} + \beta \tau_{\mathbf{r}'\mathbf{r}} t)} d\mathbf{r}. \tag{18}$$

From the Fourier transform of $s_{\mathbf{r}'}(t)$, i.e., $S_{\mathbf{r}'}(f)$, we can get a data sample at the antenna location $\mathbf{r}'$ as

$$S_{\mathbf{r}'}(\beta \tau_{\mathbf{r}'\mathbf{r}}) = \int_{\mathbf{r}} \sigma_{\mathbf{r}} e^{j2\pi f_c \tau_{\mathbf{r}'\mathbf{r}}} d\mathbf{r}, \tag{19}$$

which is just the data sample in (2).

For pulse radar or passive radar that uses communication signals, the transmitted signal can be written as $p(t) = b(t)e^{j2\pi f_c t}$, $0 \le t \le T$, where $b(t)$ is the normalized baseband pulse with duration T. The received signal (1) is now

$$\hat{s}_{\mathbf{r}'}(t) = \int_{\mathbf{r}} \sigma_{\mathbf{r}} b(t - \tau_{\mathbf{r},'\mathbf{r}}) e^{j2\pi f_c(t - \tau_{\mathbf{r},'\mathbf{r}})} d\mathbf{r}. \tag{20}$$

The receiver first removes carrier f_c and then conducts matched filtering with $b(T - t)$, which gives

$$s_{\mathbf{r}'}(t) = \int_{\mathbf{r}} \sigma_{\mathbf{r}} e^{j2\pi f_c \tau_{\mathbf{r}'\mathbf{r}}} \int b^*(z - \tau_{\mathbf{r}'\mathbf{r}}) b(T - t - z) dz d\mathbf{r}, \tag{21}$$

where * denotes conjugation. We get a data sample at the antenna position $\mathbf{r}'$ as

$$s_{\mathbf{r}'}(T + \tau_{\mathbf{r}'\mathbf{r}}) = \int_{\mathbf{r}} \sigma_{\mathbf{r}} e^{j2\pi f_c \tau_{\mathbf{r}'\mathbf{r}}} d\mathbf{r}, \tag{22}$$

which is just (2).

References

[1] B. Paul, A. R. Chiriyath, and D. W. Bliss, "Survey of RF communications and sensing convergence research," *IEEE Access*, vol. 5, pp. 252–270, 2016.

[2] A. Hassanien, M. G. Amin, Y. D. Zhang, and F. Ahmad, "Signaling strategies for dual-function radar communications: An overview," *IEEE Aerosp. Electron. Syst. Mag.*, vol. 31, no. 10, pp. 36–45, Oct. 2016.

[3] K. V. Mishra, M. B. Shankar, V. Koivunen, B. Ottersten, and S. A. Vorobyov, "Toward millimeter-wave joint radar communications: A signal processing perspective," *IEEE Signal Process. Mag.*, vol. 36, no. 5, pp. 100–114, Sep. 2019.

[4] L. Zheng, M. Lops, Y. C. Eldar, and X. Wang, "Radar and communication coexistence: An overview: A review of recent methods," *IEEE Signal Process. Mag.*, vol. 36, no. 5, pp. 85–99, Sep. 2019.

[5] I. Bilik, O. Longman, S. Villeval, and J. Tabrikian, "The rise of radar for autonomous vehicles: Signal processing solutions and future research directions," *IEEE Signal Process. Mag.*, vol. 36, no. 5, pp. 20–31, Sep. 2019.

[6] J. Choi, V. Va, N. Gonzalez-Prelcic, R. Daniels, C. R. Bhat, and R. W. Heath, "Millimeter-wave vehicular communication to support massive automotive sensing," *IEEE Commun. Mag.*, vol. 54, no. 12, pp. 160–167, Dec. 2016.

[7] P. Kumari, J. Choi, N. González-Prelcic, and R. W. Heath, "IEEE 802.11ad-based radar: An approach to joint vehicular communication-radar system," *IEEE Trans. Veh. Technol.*, vol. 67, no. 4, pp. 3012–3027, Apr. 2018.

[8] S. Z. Gurbuz and M. G. Amin, "Radar-based human-motion recognition with deep learning: Promising applications for indoor monitoring," *IEEE Signal Process. Mag.*, vol. 36, no. 4, pp. 16–28, Jul. 2019.

[9] H. Jiang, C. Cai, X. Ma, Y. Yang, and J. Liu, "Smart home based on wifi sensing: A survey," *IEEE Access*, vol. 6, pp. 13 317–13 325, 2018.

[10] J. Le Kernec *et al.*, "Radar signal processing for sensing in assisted living: The challenges associated with real-time implementation of emerging algorithms," *IEEE Signal Process. Mag.*, vol. 36, no. 4, pp. 29–41, Jul. 2019.

[11] F. Adib and D. Katabi, "See through walls with WiFi!" in *Proc. ACM Conf. SIGCOMM*, 2013, pp. 75–86.

[12] K. Chetty, G. E. Smith, and K. Woodbridge, "Through-the-wall sensing of personnel using passive bistatic wifi radar at standoff distances," *IEEE Trans. Geosci. Remote Sens.*, vol. 50, no. 4, pp. 1218–1226, Apr. 2012.

[13] J. J. Salerno, E. P. Blasch, M. Hinman, and D. M. Boulware, "Evaluating algorithmic techniques in supporting situation awareness," in *Proc. SPIE – Int. Soc. Opt. Eng.*, 2005, pp. 96–104.

[14] N. E. Alexander *et al.*, "TeraSCREEN: Multi-frequency multi-mode terahertz screening for border checks," *Passive Active Millimeter-Wave Imag. XVII*, vol. 9078, 2014, Art no. 907802.

[15] K. B. Cooper, R. J. Dengler, N. Llombart, B. Thomas, G. Chattopadhyay, and P. H. Siegel, "Thz imaging radar for standoff personnel screening," *IEEE Trans. THz Sci. Technol.*, vol. 1, no. 1, pp. 169–182, Sep. 2011.

[16] M. McCann and M. Unser, *Biomedical Image Reconstruction: From the Foundations to Deep Neural Networks* (Foundations and Trends in Signal Processing). Delft, The Netherlands: Now Publishers, 2019.

[17] F. García-Rial, D. Montesano, I. Gómez, C. Callejero, F. Bazus, and J. Grajal, "Combining commercially available active and passive sensors into a millimeter-wave imager for concealed weapon detection," *IEEE Trans. Microw. Theory Techn.*, vol. 67, no. 3, pp. 1167–1183, Mar. 2019.

[18] D. M. Sheen, D. L. McMakin, and T. E. Hall, "Three-dimensional millimeter-wave imaging for concealed weapon detection," *IEEE Trans. Microw. Theory Techn.*, vol. 49, no. 9, pp. 1581–1592, Sep. 2001.

[19] A. Fitwi, Y. Chen, and S. Zhu, "PriSe: Slenderized privacy-preserving surveillance as an edge service," in *Proc. IEEE 6th Int. Conf. Collaboration Internet Comput.*, 2020, pp. 125–134.

[20] S. Y. Nikouei, R. Xu, D. Nagothu, Y. Chen, A. Aved, and E. Blasch, "Real-time index authentication for event-oriented surveillance video query using blockchain," in *Proc. IEEE Int. Smart Cities Conf.*, 2018, pp. 1–8.

[21] S. S. Ahmed, A. Schiessl, and L.-P. Schmidt, "A novel fully electronic active real-time imager based on a planar multistatic sparse array," *IEEE Trans. Microw. Theory Techn.*, vol. 59, no. 12, pp. 3567–3576, Dec. 2011.

[22] W. F. Moulder *et al.*, "Development of a high-throughput microwave imaging system for concealed weapons detection," in *Proc. IEEE Int. Symp. Phased Array Syst. Technol.*, 2016, pp. 1–6.

[23] M. E. Yanik and M. Torlak, "Near-field MIMO-SAR millimeter-wave imaging with sparsely sampled aperture data," *IEEE Access*, vol. 7, pp. 31 801–31 819, 2019.

[24] J. Gollub *et al.*, "Large metasurface aperture for millimeter wave computational imaging at the human-scale," *Sci. Rep.*, vol. 7, no. 1, pp. 1–9, 2017.

[25] M. A. Richards, J. Scheer, W. A. Holm, and W. L. Melvin, *Principles of Modern Radar*. Citeseer, 2010.

[26] M. Radermacher, "Weighted back-projection methods," *Electron Tomography*. Berlin, Germany: Springer, 2007, pp. 245–273.

[27] L. M. Ulander, H. Hellsten, and G. Stenstrom, "Synthetic-aperture radar processing using fast factorized back-projection," *IEEE Trans. Aerosp. Electron. Syst.*, vol. 39, no. 3, pp. 760–776, Jul. 2003.

[28] M. Di Bisceglie, M. Di Santo, C. Galdi, R. Lanari, and N. Ranaldo, "Synthetic aperture radar processing with GPGPU," *IEEE Signal Process. Mag.*, vol. 27, no. 2, pp. 69–78, Mar. 2010.

[29] S. Patole and M. Torlak, "Two dimensional array imaging with beam steered data," *IEEE Trans. Image Process.*, vol. 22, no. 12, pp. 5181–5189, Dec. 2013.

[30] S. S. Haykin, *Adaptive Filter Theory*. Pearson Education India, 2008.

[31] A. Hore and D. Ziou, "Image quality metrics: PSNR vs. SSIM," in *Proc. 20th Int. Conf. Pattern Recognit.*, 2010, pp. 2366–2369.